
Comparison of Methods to Quantitate ^{18}F -FDG Uptake with PET During Experimental Acute Lung Injury

Delphine L. Chen, MD^{1,2}; Mark A. Mintun, MD¹; and Daniel P. Schuster, MD^{1,3}

¹Department of Radiology, Washington University School of Medicine, St. Louis, Missouri; ²Department of Surgery, Washington University School of Medicine, St. Louis, Missouri; and ³Department of Internal Medicine, Washington University School of Medicine, St. Louis, Missouri

PET with ^{18}F -FDG may be useful for quantifying neutrophilic activation. We previously demonstrated that pulmonary neutrophil sequestration could be detected during acute lung injury (ALI), even without migration into the alveolar compartment. Using the influx constant K_i as the method to quantify lung ^{18}F -FDG uptake, we also showed that K_i correlated positively with in vitro assays of ^3H -deoxyglucose (^3H -DG) uptake in cells harvested via bronchoalveolar lavage. In the present study, we have reanalyzed data from that study to determine if simpler nonkinetic methods of quantifying the pulmonary uptake of ^{18}F -FDG could be as powerful as calculating K_i . **Methods:** ^{18}F -FDG uptake was quantified as K_i , calculated by 3-compartmental model analysis (used as the gold standard) and Patlak graphical analysis, with and without normalization for initial volume of tracer distribution; the standardized uptake value; and the tissue-to-plasma activity ratio (TPR). **Results:** Values for K_i , determined either from a 3-compartmental model analysis of the time-activity data or by Patlak graphical analysis, were highly correlated ($R^2 = 0.97$). The correlation was worse if these variables were normalized for the initial volume of tracer distribution. TPR was highly correlated with K_i determined by the compartmental model ($R^2 = 0.96$) and with in vitro measurements of ^3H -DG uptake ($R^2 = 0.63$). **Conclusion:** The TPR is a simple and equally effective alternative to dynamic imaging in determining net ^{18}F -FDG uptake during ALI. Normalization of the kinetic data for differences in the initial volume of tracer distribution does not contribute significantly to signal interpretation during ALI.

Key Words: FDG; compartmental model; acute lung injury; inflammation imaging; PET

J Nucl Med 2004; 45:1583–1590

In recent years, PET imaging with ^{18}F -FDG has become a mainstay for the diagnosis and management of cancer. However, potential new applications for ^{18}F -FDG PET imaging continue to be explored, including a role in inflam-

mation imaging (1,2). Using a visual assessment of ^{18}F -FDG uptake, several recent studies have shown that ^{18}F -FDG PET imaging may be useful in detecting inflammation due to infection (3–5). Other studies suggest that although quantitation may not be necessary for distinguishing infectious foci from malignant lesions (6), it may enable differentiation of acute from chronic active infectious lesions (7).

Recently, we showed that ^{18}F -FDG PET imaging may be a useful tool to study the kinetics (onset, magnitude, duration) of neutrophilic activation during acute lung injury (ALI) (8). In that study, the lung uptake of ^{18}F -FDG, quantified as the influx constant K_i (calculated by Patlak graphical analysis) (9,10), was used to detect the sequestration and influx of activated neutrophils into the lungs during ALI. In addition, we showed that neutrophil activation, not nonspecific leak of ^{18}F -FDG into the air spaces, was the primary determinant of the imaging signal.

The issue of how best to quantify ^{18}F -FDG PET uptake in the lungs is important because basal uptake of glucose by the lungs, compared with other organs such as heart and brain, is very low, and a significant portion of the lung activity simply represents activity within the pulmonary blood pool. These conditions make it difficult to identify changes in pulmonary uptake of ^{18}F -FDG visually. No studies to date, however, have systematically compared available methods of quantifying ^{18}F -FDG PET imaging during acute inflammation or ALI.

Compartmental modeling of time-activity data obtained during ^{18}F -FDG PET imaging—generally considered the gold standard against which other methods are compared (11–13)—can be used to estimate rate constants that define the movement of ^{18}F -FDG between the blood and tissue compartments. An analysis of these data may also allow one to determine which steps limit the rate of ^{18}F -FDG uptake into a specific tissue (11).

A simplified but related method is the graphical analytic approach originally described by Patlak et al. (9,10). This method allows one to calculate the overall net rate of ^{18}F -FDG uptake (often referred to as the net influx constant K_i). Patlak analysis, however, depends on certain assump-

Received Dec. 28, 2003; revision accepted Mar. 4, 2004.

For correspondence or reprints contact: Delphine L. Chen, MD, Campus Box 8225, Washington University School of Medicine, 660 S. Euclid Ave., St. Louis, MO 63110.

E-mail: chend@mir.wustl.edu

tions being met, including equilibrium being reached between the blood and tissue compartments and complete entrapment of the tracer without loss (in this case, by de-phosphorylation) from the tissue region of interest (ROI) during the scan period.

The standardized uptake value (SUV) is perhaps the most widely used method of quantifying ^{18}F -FDG tissue uptake in general, including studies of inflammation imaging (2). The SUV is simply the radioactivity measured in a tissue region corrected for the dose of radioactivity injected and for body mass. In a related approach, regional tissue activity can be normalized to blood activity at the time of the scan (14).

Finally, Jones et al. introduced the concept of correcting rates of ^{18}F -FDG uptake in the lungs, as calculated by Patlak graphical analysis, for differences in the initial volume of distribution of ^{18}F -FDG (15,16). The intercept component of the linear regression used to calculate the influx constant from a Patlak plot represents this initial volume of distribution in both the tissue and the blood. Such a correction could be especially relevant in the lungs because lung "tissue" on PET images includes air and blood as well as the parenchymal tissue itself. Changes in density due to atelectasis, pulmonary edema, or inflammatory recruitment of cells might therefore alter the volume of distribution of ^{18}F -FDG and its subsequent rate of uptake.

The purpose of this study, then, was to compare these various methods for quantifying ^{18}F -FDG uptake in the lungs against the gold standard of compartmental modeling, specifically in the setting of ALI.

MATERIALS AND METHODS

The animal preparation, study design, and implementation of these experiments has been described in detail elsewhere (8) and will be described briefly here. The main focus of this study is a reanalysis of the imaging data as a comprehensive comparison of different approaches to quantifying the uptake of ^{18}F -FDG into the lungs during ALI.

Animal Preparation and Experimental Groups

The protocol for these studies was approved by the Animal Studies Committee at Washington University School of Medicine. Studies were performed on 24 healthy adult male mongrel dogs. Animals were divided into 4 groups: (a) a normal control group that received no experimental interventions ($n = 5$), (b) a group with lung injury induced by 0.08 mL/kg of oleic acid (OA) diluted in 1.5 mL of 70% ethanol (OA group, $n = 6$), (c) a group treated with 15 $\mu\text{g}/\text{kg}$ of endotoxin (Etx) (Etx group, $n = 6$), and (d) a group with lung injury induced by OA preceded by treatment with the same dose of Etx (Etx+OA group, $n = 7$). The injury model was implemented by giving either Etx or placebo intravenously first, followed 30 min later by either OA or placebo. Animals were sedated using an intravenous pentobarbital sodium infusion, intubated, and mechanically ventilated with a Harvard pump respirator using a tidal volume of 15 mL/kg and a fraction of inspired oxygen (FIO_2) of 1.0. An intravenous catheter was placed in the femoral vein for drug and radionuclide administration.

PET Data Acquisition

The same scanning protocol was used in all animals. All data were acquired using 2-dimensional mode on an ECAT EXACT HR+ scanner, and all images were reconstructed using filtered backprojection. Scatter correction was performed by deconvolving the measured projection data using a spatially invariant kernel (17); scatter contribution to the data was negligible. A 15-min attenuation scan was done initially, 1.5 h after experimental treatments were initiated, with placement of the animal such that the most caudal slice was approximately at the dome of the diaphragm. After completing the transmission scan, the following scans were obtained:

- Blood volume (BV) was determined using ^{15}O -labeled CO (C^{15}O). The animal was disconnected from the ventilator, and $\sim 1,480$ MBq (~ 40 mCi) C^{15}O were administered via a bag respirator in 2 breaths through the endotracheal tube. Two minutes later, a 5-min scan was performed.
- Lung water concentration (LWC) was determined using ^{15}O -labeled water (H_2^{15}O) by methods previously described (8). A 5-min scan was performed 3 min after intravenous injection of $\sim 1,665$ – $1,850$ MBq (45–50 mCi) H_2^{15}O to allow equilibration of the radiolabeled water between the lung tissue and blood compartments.
- ^{18}F -FDG (181 ± 19 MBq [4.9 ± 0.5 mCi]) was injected intravenously at the start of a 58-min period of dynamic scan acquisition with the following protocol: twenty 5-s, six 30-s, six 60-s, four 120-s, and eight 300-s imaging frames. One-milliliter blood samples were drawn manually from a pulmonary artery catheter according to the following schedule: every 30 s for the first 2 min, every minute for the next 8 min, every 5 min for the next 20 min, then every 10 min for the remaining 30 min, with 2 blood samples drawn at the end of the scan. Activity in 200 μL of the plasma portion was measured in a γ -counter calibrated to the PET scanner. The data from these samples were used to determine the input function for compartmental modeling of the ^{18}F -FDG time-activity data and for the Patlak graphical analysis.

PET Data Analysis

ROIs were drawn on 5 slices (slice thickness = 0.24 cm, spaced 0.95 cm apart) of the PET scans, using the transmission and lung water scans to define the lung borders (8). These ROIs were then used for all analyses.

The SUV was calculated from activity data obtained during the last frame of the ^{18}F -FDG scans as:

$$\text{SUV} = \frac{\text{tissue activity } (\mu\text{Ci}/\text{mL lung})}{\text{injected dose (mCi)/body weight (kg)}} \quad \text{Eq. 1}$$

The tissue-to-plasma activity ratio (TPR) was calculated by dividing the tissue activity data during this same last imaging frame by the radioactivity in the plasma determined from the mean of 2 blood samples obtained at the end of that frame period.

The Patlak influx constant (Patlak K_i) was obtained from a plot constructed from an area-weighted average of activity in the ROIs and the activity of ^{18}F -FDG in plasma, measured from blood samples. Linear regression was performed on all data points after 10 min of scanning with visual confirmation of linearity. All regressions had a correlation of determination (R^2) of 0.92 or greater. K_i was calculated from the slope of the equation generated by the regression. Examples of Patlak curves from these experi-

ments are presented elsewhere (8). The following equation was used to construct the Patlak plots and to generate the linear regressions:

$$\frac{C_T(t)}{C_A(t)} = \text{Patlak } K_i \times \frac{\int_0^t C_A(\tau) d\tau}{C_A(t)} + \text{Int}, \quad \text{Eq. 2}$$

where $C_T(t)$ and $C_A(t)$ are, respectively, tissue and blood radioactivity at each sample time point (t); τ is the integration variable; K_i is the Patlak influx constant; and Int is a parameter representing the initial volume of distribution of the tracer in both the tissue and blood (the intercept when plotted graphically).

The Patlak K_i was expressed simply as K_i and as K_i normalized for the initial volume of distribution (K_i/Int).

The kinetics of ^{18}F -FDG uptake in the lungs were also analyzed with a standard 3-compartmental model using nonlinear regression (18), where K_1 is the forward rate constant between the blood and tissue compartment, k_2 is the reverse rate constant between the same 2 compartments, and k_3 is the rate constant representing trapping of ^{18}F -FDG intracellularly after phosphorylation by hexokinase. Model parameters were obtained by fitting the experimental time-activity data to the following equation:

$$C_T(t) = \frac{K_1}{\alpha_2 - \alpha_1} \times [(k_3 + k_4 - \alpha_1)e^{-\alpha_1 t} + (\alpha_2 - k_3 - k_4)e^{-\alpha_2 t}] \otimes C_A(t) + \text{BV } C_A(t), \quad \text{Eq. 3}$$

where $\alpha_{2,1} = 1/2(k_2 + k_3 + k_4 \pm \sqrt{(k_2 + k_3 + k_4)^2 - 4k_2k_4})$, \otimes is the convolution operator, BV is the estimated blood volume component, and K_1 , k_2 , k_3 , and k_4 represent the individual rate constants.

It was assumed that dephosphorylation in the lungs is negligible over the 1-h scanning period, so k_4 was set to 0 and dropped from the equation. K_1 , k_2 , k_3 , and BV were then estimated by nonlinear regression using 0.04, 0.04, and 0.03 as initial estimates for the rate constants.

The influx constant K_i was also calculated from the compartmental model (CM) rate constants (9,19) as follows:

$$\text{CM } K_i \text{ (mL blood/mL lung/min)} = K_1 \frac{k_3}{(k_2 + k_3)}. \quad \text{Eq. 4}$$

The rate constants can also be used to estimate a tissue volume of distribution for the ^{18}F -FDG tracer (9,19), as follows:

$$V_t \text{ (mL/mL lung)} = K_1 \frac{k_2}{(k_2 + k_3)^2}. \quad \text{Eq. 5}$$

The compartmental model estimate of the BV was added to V_t to give the compartmental model equivalent of the Patlak intercept (9):

$$\text{CM intercept} = V_t + \text{estimated BV}. \quad \text{Eq. 6}$$

Extravascular lung water (EVLW) was calculated by the following equation (20):

$$\text{EVLW} = \text{LWC} - 0.84 \cdot \text{BV}, \quad \text{Eq. 7}$$

where LWC is the total lung water concentration obtained from the H_2^{15}O scan, BV is BV measured by the C^{15}O scan, and $0.84 \cdot \text{BV}$ is the concentration of water in the intravascular space.

Biologic Markers

After PET data acquisition, bronchoalveolar lavage (BAL) was performed by wedging a bronchoscope in a distal segment of the lung, instilling 30 mL of normal saline, and aspirating the fluid using low wall suction, sampling 2–4 different segments in each animal. Aspirated fluid was pooled and used to determine the in vitro ^3H -deoxyglucose (^3H -DG) uptake. Cells from BAL fluid were simply washed with phosphate-buffered saline (PBS) and then resuspended in Krebs–Ringer phosphate (KRP) buffer before assaying for ^3H -DG uptake. Neutrophils from blood samples taken before initiation of experimental interventions were purified as previously reported (8).

The ^3H -DG uptake assay was performed as previously described (8). Briefly, all cell pellets were washed 3 times with KRP buffer and then divided into tubes containing 5×10^5 cells per tube. One tube in each sample group was preincubated with cytochalasin B, an inhibitor of glucose uptake, to determine background ^3H -DG uptake. All tubes were then incubated with 37 kBq ^3H -DG at 37°C for 6 min and then spun down immediately at 4°C and washed with ice-cold KRP buffer 3 times. Cells were then lysed with PBS with 1% Triton X-100, cell debris was spun down, and supernatant was collected for scintillation counting and for assaying for amount of protein using the bicinchoninic acid protein assay (Pierce Technology). Results from the ^3H -DG uptake assay could be compared with PET data in only 3 of 6 dogs in the OA group and 3 of 7 dogs in the Etx+OA group, due to either insufficient cells for analysis in the BAL (6 cases) or incomplete (i.e., <1 h) PET data (1 case). The data were expressed as pmol/mg protein/min. The data from BAL cells were corrected for the percentage of neutrophils.

Statistical Tests

Group data are expressed as the mean \pm SD. Standard 1-way ANOVA tests were used to compare results among groups if data were normally distributed. Post hoc comparisons were done using the Holm–Sidak method. For non-normally distributed data, ANOVA was performed by the Kruskal–Wallis test on ranks, and subsequent post hoc comparisons were performed by the Dunn method. Statistical significance was set at $P < 0.05$. Sigma-Stat version 3.0 (SPSS, Inc.) was used for statistical testing. Nonlinear regression analyses were performed using the Levenberg–Marquardt optimization method and residuals plotted to determine goodness of fit. Bland–Altman plots were constructed to compare how well Patlak K_i values agreed with the compartmental model estimates (21).

RESULTS

Examples of time-activity data and the associated compartmental model fits from representative animals in the normal control and Etx-treated groups are shown in Figure 1. Values for the rate constants computed from the compartmental model are shown in Table 1. In general, the highest values for K_1 and k_3 were found in animals exposed to Etx. The highest mean value for K_1 was in the Etx+OA group, which was statistically different from both the normal and OA groups. The highest mean value for k_3 was in the Etx group. Mean values for k_2 were not different from one another. For all data considered as a whole, K_1 was a stronger determinant of K_i than k_3 (Fig. 2).

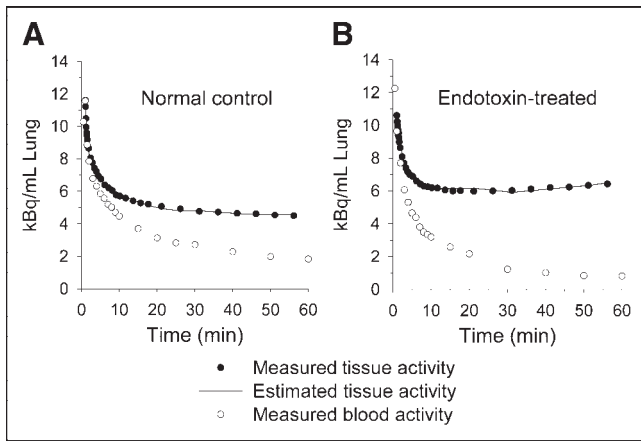


FIGURE 1. Examples of residual plots from 3-compartmental model analyses. (A) Representative plot of 1 animal in normal control group. (B) Representative plot of 1 animal in Etx-treated group. Plasma activity curve shows activity measured in plasma from direct blood sampling multiplied by fractional BV estimated by compartmental model.

K_i calculated from the estimated rate constants by compartmental modeling was highly correlated with the values of K_i calculated by Patlak analysis (Fig. 3A). A Bland-Altman plot of the K_i values (Fig. 3B) shows that there is a tendency for Patlak analysis to slightly overestimate K_i compared with the compartmental model analysis, primarily at the lower range of measured values.

Mean values for K_i both by compartmental modeling and by Patlak analysis, before and after normalization with the computed or measured intercept, are given in Table 2. Again, in general, values for normalized K_i were highest in the groups exposed to Etx. The intercept values themselves, by either method, were highest in the Etx+OA group and lowest in the normal group (Table 2). Values in the other groups were intermediate. However, the correlation between normalized K_i by the 2 methods was worse than that without the intercept correction (Fig. 3C), and though there was a tendency for the Patlak analysis to slightly overestimate normalized K_i again at lower values, there was also a

TABLE 1
Compartmental Model Rate Constants

Group	K_1	k_2	k_3
Normal	0.0049 ± 0.0020	0.070 ± 0.058	0.028 ± 0.018
OA	0.0115 ± 0.0024	0.055 ± 0.035	0.014 ± 0.009
Etx	0.0149 ± 0.0068	0.040 ± 0.018	0.049 ± 0.031*
Etx+OA	0.0339 ± 0.0071*†	0.081 ± 0.038	0.026 ± 0.016‡

* $P < 0.05$ compared with OA group.

† $P < 0.05$ compared with normal group.

‡ $P < 0.05$ compared with Etx group.

CM = compartmental model.

Units for K_1 are mL blood/mL lung/min; units for other rate constants are min^{-1} .

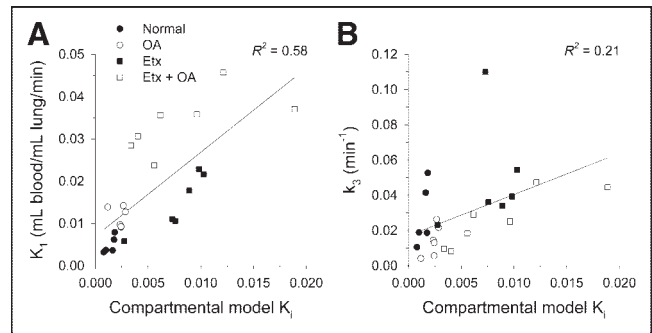


FIGURE 2. Correlations of rate constants K_1 (mL blood/mL lung/min; A) and k_3 (min^{-1} ; B) estimated by 3-compartmental model with calculated influx constant, K_i (mL blood/mL lung/min), from compartmental model. K_i represents transport of ^{18}F -FDG from vascular space into intracellular space, and k_3 represents hexokinase activity ("trapping" of ^{18}F -FDG within cell).

tendency to underestimate the normalized K_i at the higher range of measured values (Fig. 3D). The correlation of normalized K_i to ^3H -DG uptake was also worse ($R^2 = 0.48$; data not shown) when compared with our previously reported results (8).

As noted earlier, the intercept measured from the Patlak regression analysis is equivalent to the tissue volume of distribution (V_i) computed from the rate constants plus the

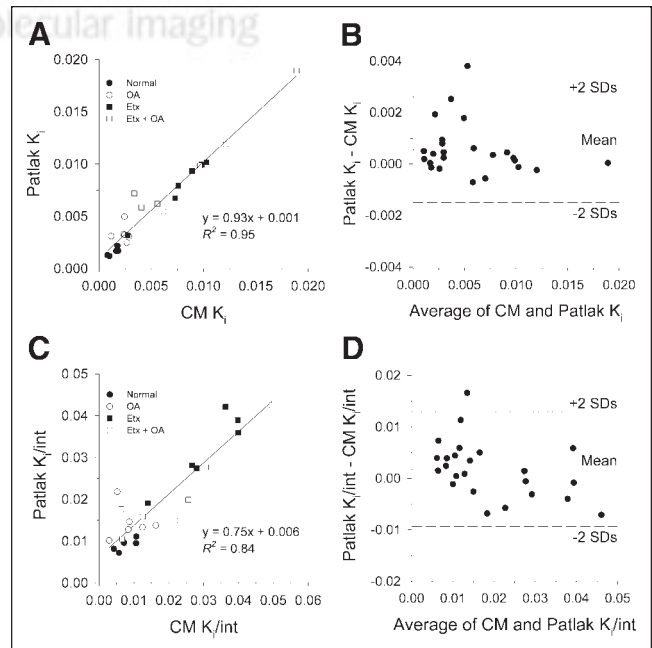


FIGURE 3. Comparisons of influx constant K_i (mL blood/mL lung/min) calculated by compartmental modeling and Patlak graphical analysis, before and after normalization for initial ^{18}F -FDG volume of distribution (int, mL/mL lung). (A) Correlation of K_i computed by the 2 methods. (B) Bland-Altman plot compares calculation of K_i values. (C) Correlation of K_i after normalization. (D) Bland-Altman plot compares normalized K_i values. Solid line shows mean value of difference in K_i estimated by the 2 methods.

TABLE 2

Comparison of Compartmental Model and Patlak Estimates of K_i , With and Without Intercept Correction, and TPR

Group	CM K_i	Patlak K_i	CM K_i /Int	Patlak K_i /Int	CM Int	Patlak Int	TPR
Normal	0.0014 ± 0.0005	0.0016 ± 0.0004	0.0077 ± 0.0029	0.0091 ± 0.0015	0.19 ± 0.04	0.18 ± 0.03	0.33 ± 0.06
OA	0.0023 ± 0.0006	0.0034 ± 0.0008	0.0090 ± 0.0049	0.0144 ± 0.0039	0.31 ± 0.11*	0.24 ± 0.04	0.62 ± 0.13
Etx	0.0078 ± 0.0027*	0.0079 ± 0.0026*	0.0308 ± 0.0100**†	0.0319 ± 0.0086*	0.26 ± 0.07	0.25 ± 0.09	1.72 ± 0.68*
Etx+OA	0.0085 ± 0.0055*	0.0093 ± 0.0048*†	0.0217 ± 0.0153	0.0213 ± 0.0107*	0.43 ± 0.11**‡	0.44 ± 0.07**‡	2.17 ± 1.48*

* $P < 0.05$ compared with normal group.

† $P < 0.05$ compared with OA group.

‡ $P < 0.05$ compared with Etx group.

CM = compartmental model.

Units for K_i are mL blood/mL lung/min; units for intercept and TPR are mL blood/mL lung.

estimated BV. These variables are compared in Table 3. There was no statistically significant difference for the mean values among the experimental groups either for the estimated pulmonary BV from the compartmental analysis or for BV measured from the $C^{15}O$ scan. In contrast, both V_t (estimated from the compartmental model analysis) and EVLW (calculated from the lung water and BV scans) were highest in the groups that developed lung injury after being exposed to OA. There was no statistically significant difference in the mean values of either variable in the Etx group versus the normal group. The Patlak intercept was strongly correlated with the calculated intercept from the compartmental model (Fig. 4A) and was more strongly correlated with V_t ($R^2 = 0.67$; data not shown) than with the compartmental model estimate of BV ($R^2 = 0.30$; data not shown). Furthermore, V_t and EVLW were positively and significantly correlated to one another (Fig. 4B).

Mean SUVs were calculated for each group. The mean SUV for the Etx+OA group (1.08 ± 0.15) was significantly higher when compared with all 3 other groups ($P < 0.05$). The mean SUV for the OA group (0.69 ± 0.11) was also significantly higher when compared with the normal group (0.45 ± 0.92 ; $P < 0.05$). The mean SUV of the Etx group

(0.61 ± 0.18) was not statistically different from the OA or normal control groups. There was a weak correlation between SUV and the K_i estimated by the compartmental model (Fig. 5). However, there was no statistically significant correlation between SUV and K_i normalized by the intercept correction by either method (unlike the modest correlation shown in Fig. 5 for the uncorrected K_i).

Mean TPR values for each group are shown in Table 2. The mean values in the Etx+OA and Etx-only groups were statistically higher than that in the normal control group. TPR was highly correlated with the compartmental model estimate of K_i (Fig. 6A) and was also positively correlated with 3H -DG uptake in neutrophils harvested from the BAL fluid (Fig. 6B).

DISCUSSION

We used compartmental modeling of the PET and blood time-activity data as the gold standard against which the different analytic methods were compared (11–13). We found that, in the current studies, modeling produced excellent fits to the observed data (Fig. 1).

TABLE 3

Comparison of Components of Compartmental Model Intercept with Independently Measured PET Variables

Group	V_t	CM BV	BV*	EVLW
Normal	0.04 ± 0.02	0.15 ± 0.02	0.16 ± 0.02	0.31 ± 0.03
OA	0.17 ± 0.10†	0.14 ± 0.03	0.21 ± 0.04	0.52 ± 0.13‡
Etx	0.09 ± 0.05	0.17 ± 0.03	0.16 ± 0.02	0.30 ± 0.03
Etx+OA	0.26 ± 0.09†§	0.17 ± 0.04	0.22 ± 0.05	0.54 ± 0.10**

*From $C^{15}O$ scan.

† $P < 0.05$ compared with normal group.

‡ $P < 0.05$ compared with Etx group.

§ $P < 0.05$ compared with OA group.

CM = compartmental model.

Units for V_t are mL blood/mL lung; BV are mL blood/mL lung; EVLW are mL H_2O /mL lung.

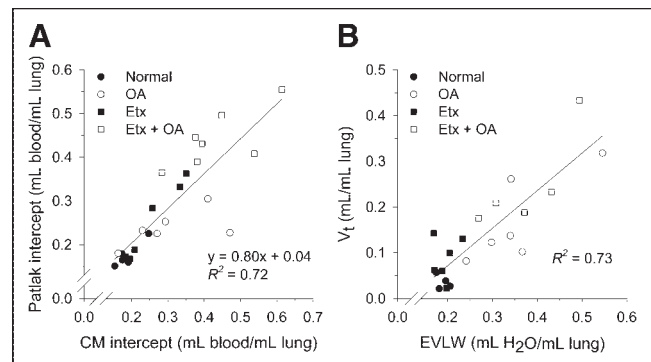


FIGURE 4. Correlations of initial ^{18}F -FDG volume of distribution in tissue (V_t) and blood (BV) calculated by compartmental model (CM intercept = $V_t + BV$) and Patlak graphical analysis and primary determinants of distribution space. (A) Correlation of CM intercept and intercept determined from Patlak linear regression. (B) Correlation of EVLW and V_t .

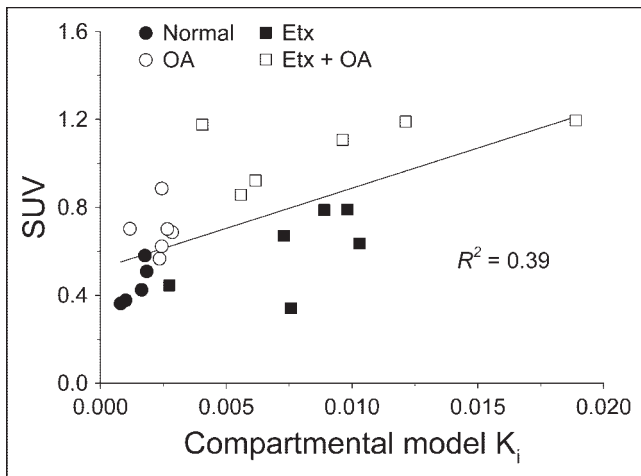


FIGURE 5. Correlation between influx constant K_i (mL blood/mL lung/min) calculated by compartmental model and SUV.

The net uptake of ^{18}F -FDG into a tissue is often summarized as the “net influx rate constant” K_i . This constant can be computed from either the compartmental model rate constants or by a graphical approach first reported by Patlak et al. (9,10). In this study, we found that the 2 methods of computing K_i correlated strongly (Fig. 3). We take this observation to indicate that the assumptions underlying the use of the Patlak approach to computing K_i are valid under our experimental conditions. As such, they strengthen the inferences drawn in our previous report concerning differences in the rate of ^{18}F -FDG uptake among the experimental groups (8).

In that report, the principal finding was that K_i increased significantly in animals exposed to Etx compared with normal animals or those exposed only to OA injury. Independent in vitro measurements of the rate of ^3H -DG uptake on cells recovered from the lungs not only supported these findings but also showed that the primary cell source of the imaging signal was the neutrophil. Thus, we interpreted the K_i measurements to indicate that the increased rate of ^{18}F -FDG uptake seen in animals exposed to Etx was primarily a function of neutrophil activation with pulmonary sequestration or infiltration into the lungs, and not from nonspecific leak of the tracer into the alveolar air spaces in the presence of ALI.

Our inferences would have been different had we adopted alternative forms of quantifying the time–activity data. For example, if we had based our interpretations on the SUV, we would have concluded that the PET signal was primarily due to the effect of OA on the lungs, implying that the combination of FDG leaking into the air spaces and inflammatory cell recruitment in response to lung injury contribute equally to the generation of the PET signal. This is clearly a different result from data obtained by compartmental modeling (Table 2).

As another example of how interpretation can be affected by the method of quantitation, Jones et al. measured the rate

of ^{18}F -FDG uptake in the lungs as K_i normalized for potential differences in the initial volume of distribution. They did this by dividing K_i by the intercept value of the linear regression used to compute K_i from the Patlak graphical approach (15,16). Presumably, the basis for their rationale in using this procedure is that the lungs, unlike other organs, can vary greatly in their tissue density. These changes in lung density could be due to atelectasis, pulmonary edema, recruitment of inflammatory cells, or some combination of these. Thus, the initial volume of distribution for the tracer could also vary widely as a result.

Without some form of validation, however, it is not intuitively obvious that this correction to the K_i measurement is appropriate. In this study, we found that the correlation between the 2 methods of K_i was worse when normalization for the intercept was used than when it was not used. Likewise, the correlation of K_i after normalization with in vitro measures of ^3H -DG uptake was worse with the intercept correction. These observations appear to indicate—in the context of these experiments involving ALI—that an intercept correction introduces additional variance into the data and is neither required nor useful.

Our analysis of the separate components of the intercept, derived from compartmental modeling, provides additional insight into why the intercept correction may not be valid in the current circumstances (i.e., during ALI). As noted in the Results, the Patlak intercept, representing V_t plus the BV, is dependent primarily on V_t (not the BV) in this model. As shown in Table 3 and Figure 4B, differences in V_t among the various experimental groups were primarily a function of changes in EVLW (i.e., pulmonary edema). Therefore, since changes in EVLW from pulmonary edema alone would not be expected to increase ^{18}F -FDG trapping, an intercept correction would artificially lower the measured rate of ^{18}F -FDG uptake. Determination of whether normalization of K_i with an intercept correction is appropriate in other pulmonary conditions associated with lung inflammation will require additional study.

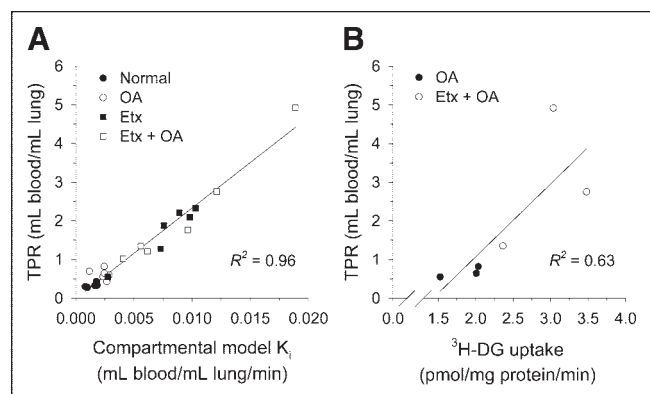


FIGURE 6. Correlation of TPR estimates to influx constant K_i (mL blood/mL lung/min) and in vitro measures of ^3H -DG uptake. (A) Correlation of TPR with compartmental model-estimated K_i . (B) Correlation of TPR with in vitro ^3H -DG uptake.

The SUV is perhaps the most common method used to quantify ^{18}F -FDG uptake. However, the SUV is influenced by factors such as the time period during which it is measured as well as the body mass (22). Accordingly, several corrections, such as standardizing the time of measurement and correcting the SUV for lean body mass or body surface area, have been proposed to reduce the dependency of the SUV on these factors (23,24). However, in the lungs and other tissues in which the rate of ^{18}F -FDG uptake is normally low, these corrections have not been effective (25). Additionally, the correlation between SUV and K_i in the current study was weak (Fig. 5). Therefore, we concluded that the SUV is not adequate for quantifying ^{18}F -FDG uptake during ALI.

As an alternative, Hunter et al. (14) proposed normalizing the tissue activity measurement at the end of the scanning period by dividing it by the measured activity in a single blood sample obtained during the time of the imaging measurement (calculating an equivalent of the TPR). They provided a theoretic justification for this approach and showed that the correlation of determination of this ratio with K_i in non-small cell lung cancer tissue was 0.98. Their findings were replicated by Krak et al. in patients with breast cancer (26). In further support of this approach, we also found that the 2 methods correlated strongly (Fig. 6A). Furthermore, TPR was linearly correlated with the in vitro measurement of ^3H -DG uptake (Fig. 6B), which was equivalent to the correlation previously reported between K_i and ^3H -DG (8).

These results have significant implications for the potential usefulness of ^{18}F -FDG PET imaging to study the kinetics (onset, magnitude, and duration) of neutrophil activation in ALI. The TPR appears to be a valid measure of ^{18}F -FDG uptake in the lungs during ALI. As such, this simplified procedure is clearly more feasible in critically ill patients than more extended scanning protocols to estimate K_i , reducing the amount of time these ventilated patients would need to be outside the intensive care unit environment. Additionally, it may be possible to calculate the TPR non-invasively by placing an ROI over the blood pool, such as in the left atrium, further simplifying the procedure (27).

Finally, if ^{18}F -FDG PET imaging is to be used to study neutrophil kinetics during ALI, it will be important to understand the regulatory mechanisms underlying glucose uptake in neutrophils. Glucose and ^{18}F -FDG both enter cells via one or more of the GLUT family of membrane transporter proteins (28,29). After phosphorylation by hexokinase, further metabolism of ^{18}F -FDG is not possible, effectively "trapping" it within the cytoplasm. Whether changes in the activity of hexokinase or the expression of the GLUT transporters is primarily responsible for the increases in ^{18}F -FDG uptake associated with Etx stimulation is not known. However, the data in Figure 2 suggest that net uptake may be more a function of transport than trapping per se. The possibility that the imaging signal during neutrophilic inflammation could be regulated by changes in

GLUT transporter expression will need to be explored in future studies.

CONCLUSION

The results of this study indicate that, during ALI, the rate of ^{18}F -FDG uptake in the lungs can be accurately estimated by use of the TPR. Normalization of the kinetic data with an intercept correction does not appear to be warranted.

ACKNOWLEDGMENTS

This work was supported by grants from the National Institutes of Health (NIH). The authors thank Jim Kozlowski, Zhaohui Zhou, Matt Bernstein, Margaret Morris, Mark Nolte, and Linda Becker for technical assistance; Bill Margenau, Dave Ficke, and the cyclotron staff for isotope production; and Marie La Regina and her staff in the Division of Comparative Medicine for assistance with specimen processing. This research was funded by NIH grants HL32815 and T32 GM08795.

REFERENCES

1. Rennen H, Boerman O, Oyen W, Corstens F. Imaging infection/inflammation in the new millennium. *Eur J Nucl Med.* 2001;28:241–252.
2. Zhuang H, Alavi A. 18-Fluorodeoxyglucose positron emission tomographic imaging in the detection and monitoring of infection and inflammation. *Semin Nucl Med.* 2002;31:47–59.
3. Stumpe K, Dazzi H, Schaffner A, von Schulthess G. Infection imaging using whole-body FDG-PET. *Eur J Nucl Med.* 2000;27:822–832.
4. Meller J, Strutz F, Siefker U, et al. Early diagnosis and follow-up of aortitis with [^{18}F]FDG PET and MRI. *Eur J Nucl Med Mol Imaging.* 2003;30:730–736.
5. Manthey N, Reinhard P, Moog F, et al. The use of [^{18}F]fluorodeoxyglucose positron emission tomography to differentiate between synovitis, loosening and infection of hip and knee prostheses. *Nucl Med Commun.* 2002;23:645–653.
6. Lowe VJ, Hoffman JM, DeLong DM, Patz EF, Coleman RE. Semiquantitative and visual analysis of FDG-PET images in pulmonary abnormalities. *J Nucl Med.* 1994;35:1771–1776.
7. Ichiya Y, Kuwabara Y, Sasaki M, et al. FDG-PET in infectious lesions: the detection and assessment of lesion activity. *Ann Nucl Med.* 1996;10:185–191.
8. Chen DL, Schuster DP. Positron emission tomography with ^{18}F -fluorodeoxyglucose to evaluate neutrophil kinetics during acute lung injury. *Am J Physiol Lung Cell Mol Physiol.* 2004;286:L834–L840.
9. Patlak CS, Blasberg RG. Graphical evaluation of blood-to-brain transfer constants from multiple-time uptake data: generalizations. *J Cereb Blood Flow Metab.* 1985;5:584–590.
10. Patlak CS, Blasberg RG, Fenstermacher JD. Graphical evaluation of blood-to-brain transfer constants from multiple-time uptake data. *J Cereb Blood Flow Metab.* 1983;3:1–7.
11. Lammertsma AA. Measurement of tumor response using [^{18}F]-2-fluoro-2-deoxy-D-glucose and positron-emission tomography. *J Clin Pharmacol.* 2001; 41(suppl):104S–106S.
12. Herrero P, Weinheimer CJ, Dence C, Oellerich WF, Gropler RJ. Quantification of myocardial glucose utilization by PET and 1-carbon-11-glucose. *J Nucl Cardiol.* 2002;9:5–14.
13. Herrero P, Sharp TL, Dence C, Haraden BM, Gropler RJ. Comparison of 1- ^{11}C -glucose and ^{18}F -FDG for quantifying myocardial glucose use with PET. *J Nucl Med.* 2002;43:1530–1541.
14. Hunter GJ, Hamberg LM, Alpert NM, Choi NC, Fischman AJ. Simplified measurement of deoxyglucose utilization rate. *J Nucl Med.* 1996;37:950–955.
15. Jones HA, Marino PS, Shakur BH, Morrell NW. In vivo assessment of lung inflammatory cell activity in patients with COPD and asthma. *Eur Respir J.* 2003;21:567–573.
16. Jones H, Sriskandan S, Peters A, et al. Dissociation of neutrophil emigration and metabolic activity in lobar pneumonia and bronchiectasis. *Eur Respir J.* 1997; 10:795–803.
17. Bergstrom M, Eriksson L, Bohm C, Blomqvist G, Litton J. Correction for

- scattered radiation in a ring detector positron camera by integral transformation of the projections. *J Comput Assist Tomogr.* 1983;7:42–50.
18. Huang SC, Phelps ME. Principles of tracer kinetic modeling in positron emission tomography and autoradiography. In: Phelps ME, Mazziotta JC, Schelbert HR, eds. *Positron Emission Tomography and Autoradiography: Principles and Applications for the Brain and Heart.* New York, NY: Raven Press; 1986:287–346.
 19. Mori K, Schmidt K, Jay T, et al. Optimal duration of experimental period in measurement of local cerebral glucose utilization with the deoxyglucose method. *J Neurochem.* 1990;54:307–319.
 20. Schuster DP, Mintun MA, Green MA, Ter-Pogossian MM. Regional lung water and hematocrit determined by positron emission tomography. *J Appl Physiol.* 1985;59:860–868.
 21. Bland JM, Altman DG. Statistical methods for assessing agreement between two methods of clinical measurement. *Lancet.* 1986;1:307–310.
 22. Keyes JW Jr. SUV: standard uptake or silly useless value? *J Nucl Med.* 1995;36:1836–1839.
 23. Schomburg A, Bender H, Reichel C, et al. Standardized uptake values of fluorine-18 fluorodeoxyglucose: the value of different normalization procedures. *Eur J Nucl Med.* 1996;23:571–574.
 24. Menda Y, Bushnell DL, Madsen MT, et al. Evaluation of various corrections to the standardized uptake value for diagnosis of pulmonary malignancy. *Nucl Med Commun.* 2001;22:1077–1081.
 25. Zasadny K, Wahl R. Standardized uptake values of normal tissues at PET with 2-[fluorine-18]-fluoro-2-deoxy-d-glucose: variations with body weight and a method for corrections. *Radiology.* 1993;189:847–850.
 26. Krak N, van der Hoeven J, Hoekstra O, et al. Measuring [¹⁸F]FDG uptake in breast cancer during chemotherapy: comparison of analytical methods. *Eur J Nucl Med Mol Imaging.* 2003;30:674–681.
 27. Bergmann SR, Herrero P, Markham J, Weinheimer CJ, Walsh MN. Noninvasive quantitation of myocardial blood flow in human subjects with oxygen-15-labeled water and positron emission tomography. *J Am Coll Cardiol.* 1989;14:639–652.
 28. Gamelli R, Liu H, He L, Hofmann C. Augmentations of glucose uptake and glucose transporter-1 in macrophages following thermal injury and sepsis in mice. *J Leukoc Biol.* 1996;59:639–647.
 29. Chakrabarti R, Jung C, Lee T, Liu H, Mookerjee B. Changes in glucose transport and transporter isoforms during the activation of human peripheral blood lymphocytes by phytohemagglutinin. *J Immunol.* 1994;152:2660–2668.

